

---

# MonoDETRNext: Next-generation Accurate and Efficient Monocular 3D Object Detection Method

---

Pan Liao, Feng Yang, Di Wu, Liu Bo,

School of Automation  
Northwestern Polytechnical University  
Xi'an, China, 710129

## Abstract

Monocular vision-based 3D object detection is crucial in various sectors, yet existing methods face significant challenges in terms of accuracy and computational efficiency. Building on the successful strategies in 2D detection and depth estimation, we propose MonoDETRNext, which seeks to optimally balance precision and processing speed. Our methodology includes the development of an efficient hybrid visual encoder, enhancement of depth prediction mechanisms, and introduction of an innovative query generation strategy, augmented by an advanced depth predictor. Building on MonoDETR, MonoDETRNext introduces two variants: MonoDETRNext-F, which emphasizes speed, and MonoDETRNext-A, which focuses on precision. We posit that MonoDETRNext establishes a new benchmark in monocular 3D object detection and opens avenues for future research. We conducted an exhaustive evaluation demonstrating the model's superior performance against existing solutions. Notably, MonoDETRNext-A demonstrated a 4.60% improvement in the  $AP_{3D}$  metric on the KITTI test benchmark over MonoDETR, while MonoDETRNext-F showed a 2.21% increase. Additionally, the computational efficiency of MonoDETRNext-F slightly exceeds that of its predecessor.

## 1 Introduction

3D object detection boasts a vast range of applications, from autonomous driving and robotic navigation to smart surveillance and virtual reality. These applications hinge critically on the precise recognition and localization of objects within 3D space. However, many 3D object detection methods often rely on expensive equipment such as LiDAR[1–6], significantly limiting their practical deployment. While several purely visual strategies have achieved notable success, these generally involve multiple cameras[7–9] and are still limited under certain circumstances. Furthermore, they typically require substantial computational power to operate effectively.

Monocular 3D detection methods have not been given much attention, largely due to their relatively low accuracy. In many scenarios that require 3D detection, it is feasible to employ LiDAR or multiple cameras, supported by top-tier computing resources. However, in extreme cases where a LiDAR or one of the cameras fails, these high-precision algorithms might be rendered ineffective. Similarly, in scenarios with restricted device availability or budget constraints, multi-view and LiDAR-dependent algorithms may not be viable. Therefore, researching monocular 3D detection algorithms holds practical significance.

In the realm of 2D detection, models from the DETR series[10–13] currently stand unmatched. MonoDETR[14] represents the first end-to-end monocular 3D object detection model within this

category. Its performance surpasses all previous monocular 3D detection approaches. However, the impressive results of MonoDETR are not sufficient to satisfy our aspirations. Introducing some of the recent advancements in technology and strategies into monocular 3D vision detection, this paper presents a new-generation model, MonoDETRNext-F.

We also observed that in MonoDETR, the acquisition of depth information is overly simplistic, which is crucial for monocular 3D detection models since depth information is one of the few available 3D data types. The accuracy of depth information is closely linked to the precision of detection. To improve depth information acquisition, we referred to established 3D depth estimation networks and designed a depth predictor that directly extracts depth information from images. We integrated this predictor with MonoDETRNext-F to develop MonoDETRNext-A, which offers enhanced detection capabilities.

Through this work, we aim to provide a significant starting point for the future development of monocular 3D vision detection models, laying a solid foundation for subsequent research and applications.

The salient innovations encapsulated within this manuscript may be delineated as follows:

- 1) Proposing two novel monocular 3D object detection models, namely MonoDETRNext-F and MonoDETRNext-A, the former adeptly balancing speed and precision, while the latter accentuates precision-centric objectives.
- 2) Architecting a hybrid vision encoder for 3D object detection, proficient in the efficient extraction of features crucial for monocular 3D object detection tasks, alongside the integration of a refined, yet lightweight depth estimation module, envisaged to bolster detection accuracy.
- 3) Drawing upon methodologies hitherto entrenched in 2D object detection paradigms, we advance a cogent strategy for object query generation tailored to the exigencies of monocular 3D object detection, underpinned by meticulously designed training strategies, aimed at optimizing model performance efficaciously.

## 2 Related Work

Current 3D object detection methods can generally be classified into two categories: camera-based methods and fusion methods integrating LiDAR and other sensors.

Camera-based methods can be further divided into monocular (single-view) and multi-view methods based on the number of input viewpoints. Monocular detectors utilize only forward-facing images as input, addressing more complex tasks with limited 2D information. Multi-view detectors simultaneously encode images of the surrounding scene, leveraging relationships between viewpoints to understand 3D space. On the other hand, fusion methods based on LiDAR and other sensor integration rely on inputs from devices such as depth cameras and LiDAR, which provide a fusion of various sensor data types, including images and point clouds. Consequently, they can acquire richer and more comprehensive depth information. Despite their higher cost, these methods typically exhibit greater robustness and accuracy in complex environments, as they can exploit the advantages of multiple sensors and integrate information from different data sources.

### 2.1 MonoDETR and other monocular 3D detection

MonoDETR [14] is a state-of-the-art method that leverages rendered transmittance to predict depth maps from a single RGB image. By capturing subtle cues in the input image, MonoDETR achieves improved accuracy and robustness to varying lighting conditions compared to traditional monocular depth estimation methods.

Several other monocular 3D reconstruction methods have been proposed in recent years. For example, MonoDTR[15] is a deep learning model that predicts depth maps from single RGB images using a transformer-based architecture. While MonoDTR achieves high accuracy, it requires additional LiDAR data for training assistance. Meanwhile, CaDDN[16] and Monorun[17] not only require LiDAR data during training but also during inference. Autoshape[18] integrates CAD data into the model to augment the restricted 3D cues. MonoDETR requires minimal 2D-3D geometric priors and does not necessitate additional annotations. Our MonoDETRNext inherits this characteristic.

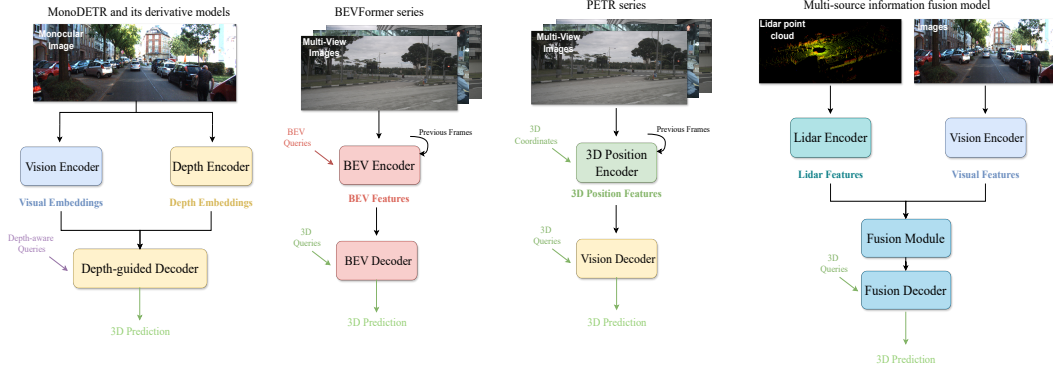


Figure 1: Comparison of mainstream 3D detection models, with different colors representing distinct functional modules.

Alternative methodologies, as demonstrated by MonoDLE [19], PGD [20], and PackNet [21], integrate multi-scale feature fusion and attention mechanisms for depth map estimation and error analysis, yielding improved performance. Despite their high accuracy, these approaches incur substantial computational costs and demand significant memory resources. Conversely, MonoDETR is characterized by its lightweight and efficient nature. Furthermore, MonoDETRNext-F surpasses it in speed and efficacy, while MonoDETRNext-A demonstrates markedly superior performance.

## 2.2 Multi-view 3D object detection

To jointly extract features from surrounding views, DETR3D [22] initially employs a set of 3D object queries, which are then back-projected onto multi-view images to aggregate features. The PETR series [23–25] further introduces the generation of 3D positional features, avoiding unstable projections, and explores the advantages of temporal information from the preceding frame.

Alternatively, BEVFormer [7] and its improvements [8, 9] generate BEV (Bird’s Eye View) features using learnable BEV queries and introduce a spatiotemporal BEV transformer for visual feature aggregation. Subsequent research has also investigated cross-modal distillation [26, 27] and masked image modeling [28, 29] to enhance performance.

## 2.3 LiDAR and multi-source information fusion 3D object detection

Methods such as DeepFusion [30] and PointPainting [31] represent notable advancements in the integration of LiDAR point cloud data with camera imagery to facilitate precise object detection within three-dimensional spatial environments. This fusion strategy optimally exploits the synergies inherent in disparate sensor modalities, amalgamating spatial depth cues with color texture information, thereby fortifying the resilience and accuracy of detection outcomes.

The integration of principles from BEVFormer into fusion paradigms, exemplified by BevFusion [6], has spurred further refinements culminating in enhanced precision, as evidenced by exemplar models such as those delineated in MV2D [4] and Futr3d [32]. Recent endeavors, typified by mmFusion [33], have expanded the purview of fusion methodologies by integrating data from multiple sensors, including cameras, LiDAR, and radar, resulting in notable performance strides.

Concurrently, the domain has witnessed the emergence of large-scale architectures, exemplified by OMNI3D [34] and GLEE [35], which have showcased remarkable efficacy in 3D object detection tasks. Leveraging copious training data and sophisticated model architectures characterized by billions of parameters or more, these frameworks have been trained utilizing advanced optimization algorithms, thereby augmenting detection performance and precision.

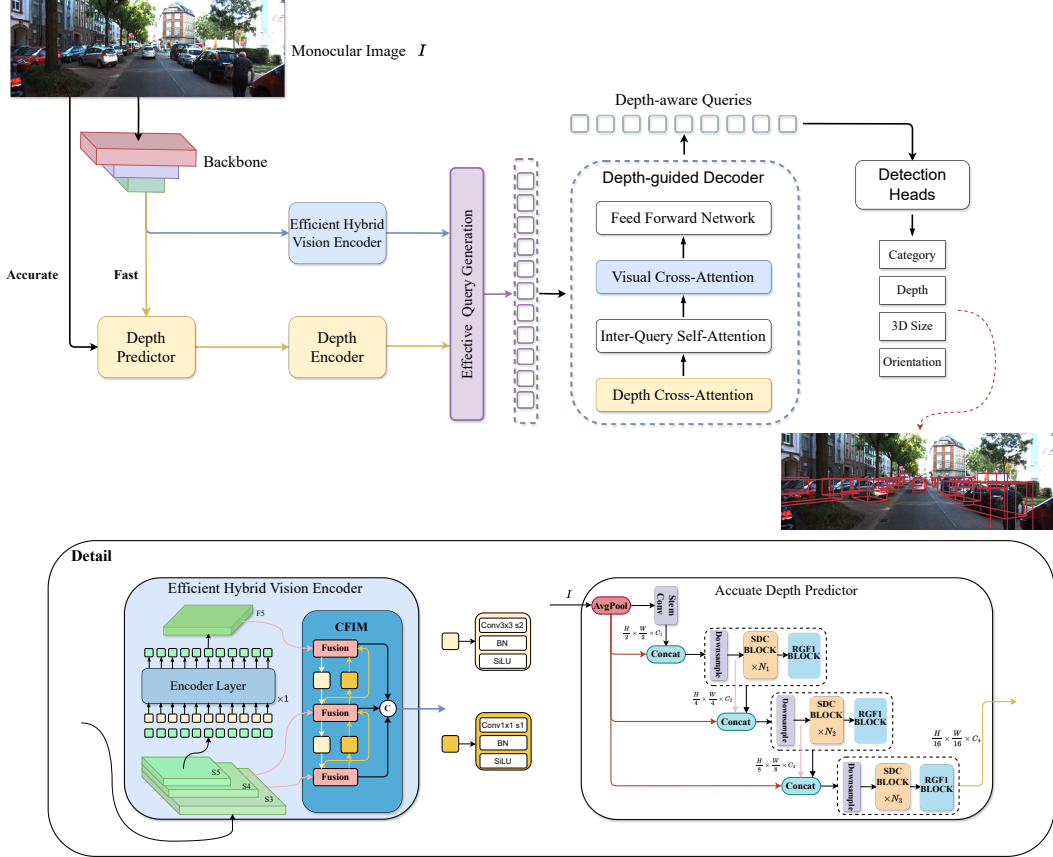


Figure 2: **The schematic depiction of MonoDETRNext.** The distinction between MonoDETRNext-A and MonoDETRNext-F primarily resides in their respective depth prediction mechanisms. The provided illustration delineates the intricate depth prediction scheme adopted by MonoDETRNext-A, whereas the depth predictor employed in MonoDETRNext-F remains congruent with that of MonoDETR.

### 3 Method

#### 3.1 Model Overview

The overall frameworks of MonoDETRNext-A and MonoDETRNext-F are illustrated in Figure 2. The main difference between these two models lies in the disparity of the depth predictors, which will be elaborated in Section 3.3. In Section 3.2, the design principles of the efficient encoder and the extraction of visual and depth features will be explicated. Lastly, in Section 3.4, the meticulous generation of object queries and the loss utilized will be expounded.

#### 3.2 Efficient Hybrid Vision Encoder

As per the findings presented in [36], the Deformable-DETR[37] allocates 49% of its computational workload to the encoder, yet this component only contributes 11% to the Average Precision (AP) metric.

Inspired by the architecture of RT-DETR[38], we introduce an innovative Efficient Hybrid Vision Encoder tailored specifically for 3d object detection tasks. This encoder is characterized by a diminished computational footprint while preserving the efficacy of feature extraction. Illustrated in Figure 2, our proposed encoder comprises two integral elements: a singular encoder layer and a Cross-Scale Feature Integration Module (CFIM) grounded in CNN. The CFIM functions as a fusion unit, amalgamating adjacent features into novel representations, as delineated in Figure 3. This fusion

process is succinctly formalized by the ensuing equations:

$$\begin{aligned}
 \mathbf{Q} &= \mathbf{K} = \mathbf{V} = \text{Flatten}(S_5) \\
 F_5 &= \text{Reshape}(\text{Attn}(\mathbf{Q}, \mathbf{K}, \mathbf{V})) \\
 \text{Output} &= \text{CFIM}(\{S_3, S_4, F_5\})
 \end{aligned} \tag{1}$$

Compared to the hybrid encoder of RT-DETR, our hybrid encoder exhibits significant differences in the Fusion module.

### 3.3 Accurate Depth Predictor

The principal disparity between our proposed models, MonoDETRNext-A and MonoDETRNext-F, resides in their Depth Predictor architecture. The initial Depth Predictor in MonoDETR, by design, featured a lightweight configuration comprising solely two 3 convolutional layers, extracting  $f_D \in \mathbb{R}^{\frac{H}{16} \times \frac{W}{16} \times (C)}$  from features preprocessed by the backbone. The accuracy of monocular 3D object detection correlates significantly with the quality of depth information obtained. In pursuit of refined depth estimation and subsequent enhancement of 3D detection precision, we undertook a redesign of the Depth Predictor. The revamped depth predictor now directly leverages the image data itself to extract depth-related features, circumventing secondary processing of backbone-derived features, thereby alleviating the potential for misalignment learning during model training.

The architectural of this novel Depth Predictor draws inspiration from several state-of-the-art monocular depth estimation models, such as lite-mono[39] and monodepth2[40]. Its specific structural configuration, as depicted in Figure 2, initiates with the processing of images of dimensions  $H \times W \times 3$  through a convolutional perturbation module, where image data undergoes downsampling via a  $3 \times 3$  convolutional operation. Subsequently, two additional  $3 \times 3$  convolutional layers, each with a stride of 1, are deployed for local feature extraction, yielding feature maps of dimensions  $\frac{H}{2} \times \frac{W}{2} \times C_1$ . In the ensuing stage, these features are concatenated with the pooled three-channel input image, followed by another downsampling step through a  $3 \times 3$  convolutional layer with a stride of 2, resulting in feature maps of dimensions  $\frac{H}{4} \times \frac{W}{4} \times C_2$ . The integration of features with the pooled input image in the downsampling layers serves to mitigate the loss of spatial information attributable to the reduction in feature dimensions, drawing inspiration from ESPNetv2[41]. Subsequent to this, RGFI and SDC are introduced to facilitate the acquisition of rich hierarchical feature representations. The ensuing downsampling layers also inherit connected features from the preceding downsampling layer. Analogously, the output feature maps undergo further processing until their dimensions align with those of MonoDETR[14], specifically  $\frac{H}{16} \times \frac{W}{16} \times C_4$ .

It is worth mentioning that MonoDETRNext-A utilizes our custom-designed Depth Predictor, while MonoDETRNext-F utilizes the original MonoDETR. After obtaining  $f_D$ , the subsequent operations for both our models, as well as MonoDETR, involve encoding through a linear classification layer and an encoder layer to obtain  $D_{fg} \in \mathbb{R}^{\frac{H}{16} \times \frac{W}{16} \times (k+1)}$  along with other additional data. These data are then fed into the depth-guided decoder to parse features.

**The Sequential Dilated Convolution (SDC)** module is introduced to extract multi-scale local features using dilated convolutions. Similar to lite-mono, we adopt a staged approach by inserting multiple consecutive dilated convolutions with varying dilation rates to effectively aggregate multi-scale context.

Given a 2D signal  $x[i]$ , the output  $y[i]$  of a 2D dilated convolution can be defined as:

$$y[i] = \sum_{k=1}^K x[i + r \cdot k]w[k], \tag{2}$$

where  $w[k]$  is a filter of length  $K$ , and  $r$  denotes the dilation rate used for convolving the input  $x[i]$ . In standard non-dilated convolutions,  $r = 1$ . By employing dilated convolutions, the network can maintain a fixed size for the output feature map while achieving a larger receptive field. Considering an input feature  $X$  with dimensions  $H \times W \times C$ , the output  $\hat{X}$  of our SDC module is computed as follows:

$$\hat{X} = X + \text{Linear}_G(\text{Linear}(\text{BN}(\text{Conv}_r(X)))) \tag{3}$$

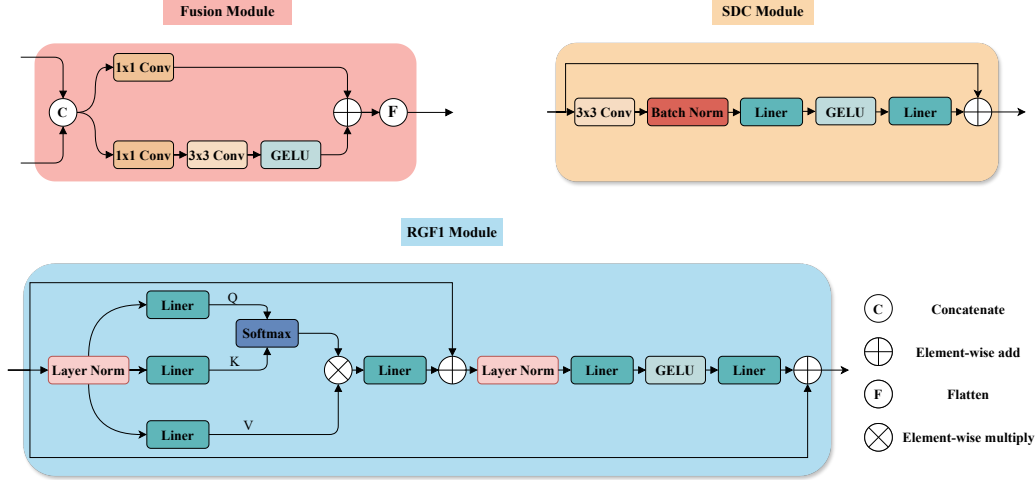


Figure 3: The fusion block within CFIM is depicted, showcasing the architectures of the Sequential Dilated Convolution (SDC) module and the Regional-Global Feature Interaction (RGFI) module proposed therein.

where  $\text{Linear}_G$  denotes pointwise convolution followed by the GELU[42] activation.  $BN$  represents the batch normalization layer, and  $\text{Conv}_r(\cdot)$  is a  $3 \times 3$  convolutional layer.

**The Regional-Global Feature Interaction (RGFI)** module operates as follows: given an input feature map  $X$  of dimensions  $H \times W \times C$ , it is linearly projected into queries  $Q = XW_q$ , keys  $K = XW_k$ , and values  $V = XW_v$ , where  $W_q$ ,  $W_k$ , and  $W_v$  are weight matrices. Cross-covariance attention[43] is employed to enhance the input  $X$ :

$$\tilde{X} = \text{Attention}(Q, K, V) + X, \quad (4)$$

Subsequently, non-linearity is introduced to enhance the features:

$$\hat{X} = X + \text{Linear}_G(\text{Linear}(\text{LN}(\tilde{X}))), \quad (5)$$

where  $LN$  represents a layer normalization[44] operation. Four variants of the depth encoder are designed based on different numbers of channels, SDC blocks. The complete process is illustrated in Figure 3.

### 3.4 Effective Query Generation and Overall Loss

In DETR, object queries are a set of learnable embeddings optimized by the decoder and mapped to classification scores and bounding boxes via prediction heads. However, these object queries are challenging to interpret and optimize as they lack explicit physical meaning. Subsequent works[45–47, 11, 48] have improved the initialization of object queries and extended them to include content queries and position queries (anchors). In 3D object detection, the position of objects is no longer a simple 2D bounding box but includes depth information in a 3D bounding box. Therefore, a more accurate and interpretable method for generating 3D object queries is needed. To address this, we introduce the process of generating object queries from 2D DETR models into 3D object detection, expanding it into depth-aware object queries.

To put it simply, we have designed a target query generation method based on the characteristics of 3D objects. In MonoDETR[14], the final output of the bbox is a six-dimensional vector,  $[x_c, y_c, x, y, w, h]$ ,  $x_c, y_c$  represent the 3D center point of the object in the image coordinates, and  $x, y, w, h$  define the 2D bbox. However, MonoDETR’s object query generates only a two-dimensional vector, which is clearly not ideal. MV2D[4] provided us with inspiration, demonstrating that 2D bounding boxes can enhance the performance of 3D detection. Therefore, we incorporated the process of generating position queries from the 2D DETR model into our system, treating the queries as bounding boxes for loss computation. Specifically, the process is as follows:

$$\begin{aligned}\mathcal{L}_{enc}(\hat{y}, y) &= \mathcal{L}_{\text{box}}(\hat{b}, b) + \mathcal{L}_{\text{cls}}(\hat{c}, \hat{b}, y, b) \\ &= \mathcal{L}_{\text{box}}(\hat{b}, b) + \mathcal{L}_{\text{cls}}(\hat{c}, c, IoU)\end{aligned}\tag{6}$$

where  $\hat{y}$  and  $y$  denote prediction and ground truth,  $\hat{y} = \hat{c}, \hat{b}$  and  $y = c, b$ ,  $c$  and  $b$  represent categories and bounding boxes, respectively. We introduce the IoU score. Additionally, we incorporate the IoU score into the classification branch’s objective function (similar to VFL[49] and RT-DETR[38]), achieving consistency constraints for positive sample classification and localization.

For generating 3D centers, we experiment with several methods, but regretfully find that a set of learnable embeddings yields the best results. Finally, our overall loss is similar to that of MonoDETR, except  $\mathcal{L}_{enc}$ :

$$\mathcal{L}_{\text{overall}} = \frac{1}{N_{gt}} \cdot \sum_{n=1}^{N_{gt}} (\mathcal{L}_{2D} + \mathcal{L}_{3D} + \mathcal{L}_{enc}) + \mathcal{L}_{\text{dmap}}\tag{7}$$

where  $\mathcal{L}_{\text{dmap}}$  represents the focal loss[50] of the predicted categorical foreground depth map  $D_{fg}$  in Section.3.3 and  $N_{gt}$  denotes the number of ground-truth objects. Additionally, it is noteworthy that the proportion of the total weight attributed to the  $\mathcal{L}_{\text{dmap}}$  loss during training differs between MonoDETRNext-A and MonoDETRNext-F, with MonoDETRNext-A having a higher percentage.

## 4 Experiments

### 4.1 Setting

#### 4.1.1 Dataset

MonoDETRNext is assessed on the extensively utilized KITTI[51] benchmark, which encompasses 7,481 training and 7,518 test images. Following the protocol outlined in previous studies [52, 53], we segregate 3,769 validation images from the training set. Evaluation is conducted across three difficulty levels: easy, moderate, and hard. Performance metrics are computed based on average precision ( $AP$ ) of bounding boxes in both 3D space ( $AP_{3D}$ ) and the bird’s-eye view ( $AP_{BEV}$ ). These metrics are assessed at 40 recall positions to ensure comprehensive evaluation.

**Note:** The reason for not using commonly used datasets for other types of 3D detection methods is that the vast majority of monocular 3D detection methods have only been validated on the KITTI, and we cannot find their results on other datasets.

#### 4.1.2 Implementation details

We employed ResNet50[54] as our backbone. While we also explored more advanced networks such as ConvNext[55], regrettably, these sophisticated architectures did not yield performance improvements. We utilized eight attention heads for all attention modules, including RGFI. MonoDETRNext-F was trained for 230 epochs on a single RTX 4090 GPU, with a batch size of 8 and a learning rate of  $2 \times 10^{-4}$ . MonoDETRNext-A was trained for 300 epochs, with the learning rate decayed between epochs 225 and 275. We employed the AdamW[56] optimizer with weight decay of  $10^{-4}$ . For MonoDETRNext-F, the learning rate was decreased by a factor of 0.1 at epochs 145 and 205 and for MonoDETRNext-A, the process is between 165 and 205. The number of object queries was consistent with MonoDETR, set at 50. Inference speed was evaluated on a single RTX 3090 GPU.

### 4.2 Comparison with SOTA

The table 1 presents a comparison of various monocular 3D object detection models on the KITTI dataset, focusing on the car category’s performance. The evaluation metrics  $AP_{3D}$  and  $AP_{BEV}$ , which are both at 40 recall positions, across different difficulty levels (Easy, Moderate, and Hard) for both the test and validation sets. Additionally, the FPS metric for batch size 1 is provided to gauge the inference speed of each model.

Among the methods listed, our methods MonoDETRNext-F and MonoDETRNext-A stands out. These variants exhibit notable advantages over other models in terms of both accuracy and efficiency.

Table 1: **Monocular performance of the car category on KITTI test and val sets.** We utilize bold numbers to highlight the best results, and color the second-best ones expect our methods and our gain over them in blue. The FPS values are obtained through speed testing conducted on individual models using a single NVIDIA GeForce RTX 3090 GPU. During testing, a batch size of 1 was utilized.

Method	$FPS_{bz=1}$	Test, $AP_{3D}$			Test, $AP_{BEV}$			Val, $AP_{3D}$		
		Easy	Mod.	Hard	Easy	Mod.	Hard	Easy	Mod.	Hard
SMOK[57]	17.6	14.03	9.76	7.84	20.83	14.49	12.75	14.76	12.85	11.50
MonoPair [58]	-	13.04	9.99	8.65	19.28	14.83	12.89	16.28	12.30	10.42
RTM3D [59]	23.3	13.61	10.09	8.18	-	-	-	19.47	16.29	15.57
PatchNet [60]	-	15.68	11.12	10.17	22.97	16.86	14.97	-	-	-
D4LCN [61]	-	16.65	11.72	9.51	22.51	16.02	12.55	-	-	-
DDMP-3D [62]	9.4	19.71	12.78	9.80	28.08	17.89	13.44	-	-	-
Kinematic3D [63]	15.6	19.07	12.72	9.17	26.69	17.52	13.10	19.76	14.10	10.47
MonoRUn [17]	20.2	19.65	12.30	10.58	27.94	17.34	15.24	20.02	14.65	12.61
CaDDN [16]	-	19.17	13.41	11.46	27.94	18.91	17.19	23.57	16.31	13.84
PGD [20]	23.9	19.05	11.76	9.39	26.89	16.51	13.49	19.27	13.23	10.65
MonoDLE [19]	25.0	17.23	12.26	10.29	24.79	18.89	16.00	17.45	13.66	11.68
MonoRCNN [64]	24.7	18.36	12.65	10.03	25.48	18.11	14.10	16.61	13.19	10.65
MonoGeo [65]	-	18.85	13.81	11.52	25.86	18.99	16.19	18.45	14.48	12.87
MonoFlex [66]	27.9	19.94	13.89	12.07	28.23	19.75	16.89	23.64	17.51	14.83
GUPNet [67]	28.7	20.11	14.20	11.77	-	-	-	22.76	16.46	13.72
MonoDTR [15]	27.0	21.99	15.39	12.73	28.59	20.38	17.14	24.52	18.57	15.51
AutoShape [18]	-	22.47	14.17	11.36	30.66	20.08	15.59	20.09	14.65	12.07
MonoDETR[14]	26.5	25.00	16.47	13.58	33.60	22.11	18.60	28.84	20.61	16.38
SSD-MonoDETR[68]	-	24.52	17.88	15.73	33.59	24.35	21.98	29.53	21.96	18.20
MonoDETRNext-F	29.2	27.21	21.69	20.16	34.56	28.12	26.31	30.28	24.77	20.38
MonoDETRNext-A	20.8	29.94	24.14	23.79	37.32	30.68	30.29	33.44	25.75	22.40

In terms of accuracy, MonoDETRNext-F achieves impressive  $AP_{3D}$  and  $AP_{BEV}$  scores across all difficulty levels, surpassing all other models listed. Specifically, it outperforms MonoDETR and SSD-MonoDETR in  $AP_{3D}$ , showcasing its superior ability to accurately detect 3D objects. Additionally, it achieves the highest  $AP_{BEV}$  scores, indicating its effectiveness in detecting objects from a bird’s eye view perspective.

MonoDETRNext-A also demonstrates competitive performance, particularly in the validation set where it achieves the highest  $AP_{3D}$  and  $AP_{BEV}$  scores among all models.

Furthermore, both MonoDETRNext-F and MonoDETRNext-A exhibit respectable inference speeds, with MonoDETRNext-F achieving the highest  $FPS_{bz=1}$  among all models.

### 4.3 Ablation Studies

We have validated the effectiveness of each component and strategy, and reported the  $AP_{3D}$  for the car category on the KITTI validation benchmark.

Our study evaluates different strategies for object query generation, as depicted in Table 2a. "L-center assign learnable embeddings," "enc-box," and "enc-center" refer to the anchors derived from backbone features, generated separately by two heads and contributing to individual loss calculation. Additionally, "enc-output" signifies six-dimensional anchors produced by a single head, also participating in loss calculation. Among these strategies, the proposed effective depth-aware query generation demonstrates notable performance, as evidenced by superior results across Easy, Moderate, and Hard stages compared to alternative methods.

Table 2b illustrates the performance of MonoDETRNext-F with different vision encoders, including the "hybrid" encoder featured in Figure 2. Notably, the "hybrid" encoder demonstrates superior performance across Easy, Moderate, and Hard categories compared to other configurations. Interestingly,



(a) Performance of MonoDETRNext-F at different 3D object query generation strategy

Stage	Easy	Mod.	Hard
L-center+enc-box	30.28	24.77	20.38
enc-center+enc-box	23.89	19.49	17.97
enc-output	23.80	18.96	16.47
w/o	22.97	17.01	15.45

(c) Effect of Different Scales of Accurate Depth Predictors on MonoDETRNext-A Performance

$N_1, N_2, N_3$	Easy	Moderate	Hard
2, 2, 4	33.44	25.75	22.40
1, 1, 2	30.26	24.99	22.58
3, 3, 6	32.45	23.85	21.85
4, 4, 6	31.78	23.56	20.78

(b) Performance of MonoDETRNext-F under different vision encoder

Model	Easy	Mod.	Hard
hybrid	30.28	24.77	20.38
hybrid-L	29.42	22.01	18.99
MonoDETR's	28.20	22.06	18.32
RT-DETR's	26.42	20.45	16.78

(d) The impact of different depth positional encodings of MonoDETRNext-F.

Settings	Easy	Mod.	Hard
3D sin/cos	30.28	24.77	20.38
2D sin/cos	28.21	21.52	18.77
Meter-wise	26.29	20.04	18.13
k-bin	25.20	18.51	16.85

Table 2: **Ablation Studies on Our Proposed MonoDETRNext on the KITTI validation benchmark.** The specific meanings of the table can be referred to in Section 4.3.

even with fewer layers, the "hybrid-L" encoder maintains competitive performance, suggesting that a lower layer count may be more effective. This observation prompts speculation: the efficacy of fewer layers could stem from the relatively limited KITTI dataset or indicate that a single layer may constitute a more rational design choice. Further analysis is warranted to discern whether this trend holds across diverse datasets and to explore potential implications for architectural design in 3d object detection tasks.

In Table 2d, the impact of different depth positional encodings on MonoDETRNext-F is examined. "3D sin/cos" and "2D sin/cos" utilize sinusoidal functions for encoding, with the former incorporating all six output dimensions. Notably, "3D sin/cos" outperforms other settings across Easy, Moderate, and Hard categories. This suggests that the precise encoding of depth information through sinusoidal functions significantly benefits object detection. Conversely, "Meter-wise" and "k-bin" positional encodings yield comparatively lower performance, indicating less effective depth representation in these configurations. Further investigation into the mechanisms behind these encoding methods is warranted to optimize depth-aware object detection algorithms.

In Table 2c,  $N_1$ ,  $N_2$ , and  $N_3$  signify the number of SDC modules, as depicted in Figure 2 .

## 5 Conclusion and Limitations

**Conclusion:** This paper introduces a novel monocular vision-based approach for 3D object detection. Leveraging advancements from the 2D detection domain, we propose the efficient and precise MonoDETRNext. Building upon the groundwork laid by MonoDETR, we introduce two variants: MonoDETRNext-F prioritizing speed, and MonoDETRNext-A emphasizing accuracy. Our methodology encompasses the development of an efficient hybrid vision encoder, enhancements to depth prediction mechanisms, and refinements in object query generation. Through comprehensive performance evaluation, we establish the superiority of our model over existing methods. By optimizing both accuracy and computational efficiency, MonoDETRNext sets a new benchmark in monocular 3D object detection, facilitating future research and applications across diverse real-world scenarios.

**Limitations:** Despite the substantial advancements achieved by MonoDETRNext in enhancing the accuracy and computational efficiency of monocular 3D object detection, certain limitations persist. Due to the inherent constraints of monocular vision methods, there remains a notable discrepancy in accuracy and performance compared to approaches employing multi-view methodologies or sensor fusion techniques, such as the integration of LiDAR with cameras.

## References

- [1] Hai Wu, Chenglu Wen, Shaoshuai Shi, Xin Li, and Cheng Wang. Virtual sparse convolution for multimodal 3d object detection. In *Proceedings of the IEEE/CVF Conference on Computer Vision and Pattern Recognition*, pages 21653–21662, 2023.
- [2] Zichao Dong, Hang Ji, Xufeng Huang, Weikun Zhang, Xin Zhan, and Junbo Chen. Pep: a point enhanced painting method for unified point cloud tasks, 2023.
- [3] Xin Li, Tao Ma, Yuenan Hou, Botian Shi, Yuchen Yang, Youquan Liu, Xingjiao Wu, Qin Chen, Yikang Li, Yu Qiao, et al. Logonet: Towards accurate 3d object detection with local-to-global cross-modal fusion. In *Proceedings of the IEEE/CVF Conference on Computer Vision and Pattern Recognition*, pages 17524–17534, 2023.
- [4] Zitian Wang, Zehao Huang, Jiahui Fu, Naiyan Wang, and Si Liu. Object as query: Lifting any 2d object detector to 3d detection. In *Proceedings of the IEEE/CVF International Conference on Computer Vision*, pages 3791–3800, 2023.
- [5] H Hu, F Wang, J Su, Y Wang, L Hu, W Fang, J Xu, and Z Zhang. Ea-lss: Edge-aware lift-splat-shot framework for 3d bev object detection. *arXiv preprint arXiv:2303.17895*, 2, 2023.
- [6] Tingting Liang, Hongwei Xie, Kaicheng Yu, Zhongyu Xia, Zhiwei Lin, Yongtao Wang, Tao Tang, Bing Wang, and Zhi Tang. Bevfusion: A simple and robust lidar-camera fusion framework. *Advances in Neural Information Processing Systems*, 35:10421–10434, 2022.
- [7] Zhiqi Li, Wenhai Wang, Hongyang Li, Enze Xie, Chonghao Sima, Tong Lu, Yu Qiao, and Jifeng Dai. Bevformer: Learning bird’s-eye-view representation from multi-camera images via spatiotemporal transformers. In *European conference on computer vision*, pages 1–18. Springer, 2022.
- [8] Chenyu Yang, Yuntao Chen, Hao Tian, Chenxin Tao, Xizhou Zhu, Zhaoxiang Zhang, Gao Huang, Hongyang Li, Yu Qiao, Lewei Lu, et al. Bevformer v2: Adapting modern image backbones to bird’s-eye-view recognition via perspective supervision. In *Proceedings of the IEEE/CVF Conference on Computer Vision and Pattern Recognition*, pages 17830–17839, 2023.
- [9] Chenbin Pan, Burhaneddin Yaman, Senem Velipasalar, and Liu Ren. Clip-bevformer: Enhancing multi-view image-based bev detector with ground truth flow. *arXiv preprint arXiv:2403.08919*, 2024.
- [10] Nicolas Carion, Francisco Massa, Gabriel Synnaeve, Nicolas Usunier, Alexander Kirillov, and Sergey Zagoruyko. End-to-end object detection with transformers. In *European conference on computer vision*, pages 213–229. Springer, 2020.
- [11] Hao Zhang, Feng Li, Shilong Liu, Lei Zhang, Hang Su, Jun Zhu, Lionel M Ni, and Heung-Yeung Shum. Dino:detr with improved denoising anchor boxes for end-to-end object detection. 2022.
- [12] Qiang Chen, Xiaokang Chen, Jian Wang, Shan Zhang, Kun Yao, Haocheng Feng, Junyu Han, Errui Ding, Gang Zeng, and Jingdong Wang. Group detr: Fast detr training with group-wise one-to-many assignment. In *Proceedings of the IEEE/CVF International Conference on Computer Vision*, pages 6633–6642, 2023.
- [13] Zhuofan Zong, Guanglu Song, and Yu Liu. Detsr with collaborative hybrid assignments training. In *Proceedings of the IEEE/CVF International Conference on Computer Vision*, pages 6748–6758, 2023.
- [14] Renrui Zhang, Han Qiu, Tai Wang, Ziyu Guo, Ziteng Cui, Yu Qiao, Hongsheng Li, and Peng Gao. Monodetr: Depth-guided transformer for monocular 3d object detection. In *Proceedings of the IEEE/CVF International Conference on Computer Vision*, pages 9155–9166, 2023.
- [15] Kuan-Chih Huang, Tsung-Han Wu, Hung-Ting Su, and Winston H Hsu. Monodtr: Monocular 3d object detection with depth-aware transformer. In *Proceedings of the IEEE/CVF Conference on Computer Vision and Pattern Recognition*, pages 4012–4021, 2022.

- [16] Cody Reading, Ali Harakeh, Julia Chae, and Steven L Waslander. Categorical depth distribution network for monocular 3d object detection. In *Proceedings of the IEEE/CVF Conference on Computer Vision and Pattern Recognition*, pages 8555–8564, 2021.
- [17] Hansheng Chen, Yuyao Huang, Wei Tian, Zhong Gao, and Lu Xiong. Monorun: Monocular 3d object detection by reconstruction and uncertainty propagation. In *Proceedings of the IEEE/CVF Conference on Computer Vision and Pattern Recognition*, pages 10379–10388, 2021.
- [18] Zongdai Liu, Dingfu Zhou, Feixiang Lu, Jin Fang, and Liangjun Zhang. Autoshape: Real-time shape-aware monocular 3d object detection. In *Proceedings of the IEEE/CVF International Conference on Computer Vision*, pages 15641–15650, 2021.
- [19] Xinzhu Ma, Yinmin Zhang, Dan Xu, Dongzhan Zhou, Shuai Yi, Haojie Li, and Wanli Ouyang. Delving into localization errors for monocular 3d object detection. In *Proceedings of the IEEE/CVF Conference on Computer Vision and Pattern Recognition*, pages 4721–4730, 2021.
- [20] Tai Wang, ZHU Xinge, Jiangmiao Pang, and Dahua Lin. Probabilistic and geometric depth: Detecting objects in perspective. In *Conference on Robot Learning*, pages 1475–1485. PMLR, 2022.
- [21] Arun Mallya and Svetlana Lazebnik. Packnet: Adding multiple tasks to a single network by iterative pruning. In *Proceedings of the IEEE conference on Computer Vision and Pattern Recognition*, pages 7765–7773, 2018.
- [22] Yue Wang, Vitor Campagnolo Guizilini, Tianyuan Zhang, Yilun Wang, Hang Zhao, and Justin Solomon. Detr3d: 3d object detection from multi-view images via 3d-to-2d queries. In *Conference on Robot Learning*, pages 180–191. PMLR, 2022.
- [23] Yingfei Liu, Tiancai Wang, Xiangyu Zhang, and Jian Sun. Petr: Position embedding transformation for multi-view 3d object detection. In *European Conference on Computer Vision*, pages 531–548. Springer, 2022.
- [24] Yingfei Liu, Junjie Yan, Fan Jia, Shuailin Li, Aqi Gao, Tiancai Wang, and Xiangyu Zhang. PetrV2: A unified framework for 3d perception from multi-camera images. In *Proceedings of the IEEE/CVF International Conference on Computer Vision*, pages 3262–3272, 2023.
- [25] Shihao Wang, Yingfei Liu, Tiancai Wang, Ying Li, and Xiangyu Zhang. Exploring object-centric temporal modeling for efficient multi-view 3d object detection. In *Proceedings of the IEEE/CVF International Conference on Computer Vision*, pages 3621–3631, 2023.
- [26] Peixiang Huang, Li Liu, Renrui Zhang, Song Zhang, Xinli Xu, Baichao Wang, and Guoyi Liu. Tig-bev: Multi-view bev 3d object detection via target inner-geometry learning. *arXiv preprint arXiv:2212.13979*, 2022.
- [27] Haimei Zhao, Qiming Zhang, Shanshan Zhao, Zhe Chen, Jing Zhang, and Dacheng Tao. Simdistill: Simulated multi-modal distillation for bev 3d object detection. In *Proceedings of the AAAI Conference on Artificial Intelligence*, volume 38, pages 7460–7468, 2024.
- [28] Jihan Yang, Shaoshuai Shi, Runyu Ding, Zhe Wang, and Xiaojuan Qi. Towards efficient 3d object detection with knowledge distillation. *Advances in Neural Information Processing Systems*, 35:21300–21313, 2022.
- [29] Anthony Chen, Kevin Zhang, Renrui Zhang, Zihan Wang, Yuheng Lu, Yandong Guo, and Shanghang Zhang. Pimae: Point cloud and image interactive masked autoencoders for 3d object detection. In *Proceedings of the IEEE/CVF Conference on Computer Vision and Pattern Recognition*, pages 5291–5301, 2023.
- [30] Yingwei Li, Adams Wei Yu, Tianjian Meng, Ben Caine, Jiquan Ngiam, Daiyi Peng, Junyang Shen, Yifeng Lu, Denny Zhou, Quoc V Le, et al. Deepfusion: Lidar-camera deep fusion for multi-modal 3d object detection. In *Proceedings of the IEEE/CVF Conference on Computer Vision and Pattern Recognition*, pages 17182–17191, 2022.

- [31] Sourabh Vora, Alex H Lang, Bassam Helou, and Oscar Beijbom. Pointpainting: Sequential fusion for 3d object detection. In *Proceedings of the IEEE/CVF conference on computer vision and pattern recognition*, pages 4604–4612, 2020.
- [32] Xuanyao Chen, Tianyuan Zhang, Yue Wang, Yilun Wang, and Hang Zhao. Futr3d: A unified sensor fusion framework for 3d detection. In *proceedings of the IEEE/CVF conference on computer vision and pattern recognition*, pages 172–181, 2023.
- [33] Javed Ahmad and Alessio Del Bue. mmfusion: Multimodal fusion for 3d objects detection. *arXiv preprint arXiv:2311.04058*, 2023.
- [34] Garrick Brazil, Abhinav Kumar, Julian Straub, Nikhila Ravi, Justin Johnson, and Georgia Gkioxari. Omni3d: A large benchmark and model for 3d object detection in the wild. In *Proceedings of the IEEE/CVF conference on computer vision and pattern recognition*, pages 13154–13164, 2023.
- [35] Junfeng Wu, Yi Jiang, Qihao Liu, Zehuan Yuan, Xiang Bai, and Song Bai. General object foundation model for images and videos at scale. *arXiv preprint arXiv:2312.09158*, 2023.
- [36] Junyu Lin, Xiaofeng Mao, Yuefeng Chen, Lei Xu, Yuan He, and Hui Xue. D<sup>2</sup>etr: Decoder-only detr with computationally efficient cross-scale attention. *arXiv preprint arXiv:2203.00860*, 2022.
- [37] Xizhou Zhu, Weijie Su, Lewei Lu, Bin Li, Xiaogang Wang, and Jifeng Dai. Deformable detr: Deformable transformers for end-to-end object detection. *arXiv preprint arXiv:2010.04159*, 2020.
- [38] Yian Zhao, Wenyu Lv, Shangliang Xu, Jinman Wei, Guanzhong Wang, Qingqing Dang, Yi Liu, and Jie Chen. Dets beat yolos on real-time object detection. *arXiv preprint arXiv:2304.08069*, 2023.
- [39] Ning Zhang, Francesco Nex, George Vosselman, and Norman Kerle. Lite-mono: A lightweight cnn and transformer architecture for self-supervised monocular depth estimation. In *Proceedings of the IEEE/CVF Conference on Computer Vision and Pattern Recognition*, pages 18537–18546, 2023.
- [40] Clément Godard, Oisín Mac Aodha, Michael Firman, and Gabriel J Brostow. Digging into self-supervised monocular depth estimation. In *Proceedings of the IEEE/CVF international conference on computer vision*, pages 3828–3838, 2019.
- [41] Sachin Mehta, Mohammad Rastegari, Linda Shapiro, and Hannaneh Hajishirzi. Espnetv2: A light-weight, power efficient, and general purpose convolutional neural network. In *Proceedings of the IEEE/CVF conference on computer vision and pattern recognition*, pages 9190–9200, 2019.
- [42] Dan Hendrycks and Kevin Gimpel. Gaussian error linear units (gelus). *arXiv preprint arXiv:1606.08415*, 2016.
- [43] Alaaeldin Ali, Hugo Touvron, Mathilde Caron, Piotr Bojanowski, Matthijs Douze, Armand Joulin, Ivan Laptev, Natalia Neverova, Gabriel Synnaeve, Jakob Verbeek, et al. Xcit: Cross-covariance image transformers. *Advances in neural information processing systems*, 34:20014–20027, 2021.
- [44] Jimmy Lei Ba, Jamie Ryan Kiros, and Geoffrey E Hinton. Layer normalization. *arXiv preprint arXiv:1607.06450*, 2016.
- [45] Feng Li, Hao Zhang, Shilong Liu, Jian Guo, Lionel M Ni, and Lei Zhang. Dn-detr: Accelerate detr training by introducing query denoising. In *Proceedings of the IEEE/CVF Conference on Computer Vision and Pattern Recognition*, pages 13619–13627, 2022.
- [46] Yingming Wang, Xiangyu Zhang, Tong Yang, and Jian Sun. Anchor detr: Query design for transformer-based detector. In *Proceedings of the AAAI conference on artificial intelligence*, volume 36, pages 2567–2575, 2022.

- [47] Shilong Liu, Feng Li, Hao Zhang, Xiao Yang, Xianbiao Qi, Hang Su, Jun Zhu, and Lei Zhang. Dab-detr: dynamic anchor boxes are better queries for detr. 2022.
- [48] Zhuyu Yao, Jiangbo Ai, Boxun Li, and Chi Zhang. Efficient detr: improving end-to-end object detector with dense prior. *arXiv preprint arXiv:2104.01318*, 2021.
- [49] Haoyang Zhang, Ying Wang, Feras Dayoub, and Niko Sunderhauf. Varifocalnet: An iou-aware dense object detector. In *Proceedings of the IEEE/CVF conference on computer vision and pattern recognition*, pages 8514–8523, 2021.
- [50] Tsung-Yi Lin, Priya Goyal, Ross Girshick, Kaiming He, and Piotr Dollár. Focal loss for dense object detection. In *Proceedings of the IEEE international conference on computer vision*, pages 2980–2988, 2017.
- [51] Andreas Geiger, Philip Lenz, and Raquel Urtasun. Are we ready for autonomous driving? The KITTI vision benchmark suite. In *2012 IEEE Conference on Computer Vision and Pattern Recognition*, pages 3354–3361, June 2012. doi: 10.1109/CVPR.2012.6248074.
- [52] Xiaozhi Chen, Kaustav Kundu, Ziyu Zhang, Huimin Ma, Sanja Fidler, and Raquel Urtasun. Monocular 3d object detection for autonomous driving. In *Proceedings of the IEEE conference on computer vision and pattern recognition*, pages 2147–2156, 2016.
- [53] Xiaozhi Chen, Kaustav Kundu, Yukun Zhu, Andrew G Berneshawi, Huimin Ma, Sanja Fidler, and Raquel Urtasun. 3d object proposals for accurate object class detection. *Advances in neural information processing systems*, 28, 2015.
- [54] Kaiming He, Xiangyu Zhang, Shaoqing Ren, and Jian Sun. Deep residual learning for image recognition. In *Proceedings of the IEEE conference on computer vision and pattern recognition*, pages 770–778, 2016.
- [55] Zhuang Liu, Hanzi Mao, Chao-Yuan Wu, Christoph Feichtenhofer, Trevor Darrell, and Saining Xie. A convnet for the 2020s. *Proceedings of the IEEE/CVF Conference on Computer Vision and Pattern Recognition (CVPR)*, 2022.
- [56] Ilya Loshchilov and Frank Hutter. Decoupled weight decay regularization. *arXiv preprint arXiv:1711.05101*, 2017.
- [57] Zechen Liu, Zizhang Wu, and Roland Tóth. Smoke: Single-stage monocular 3d object detection via keypoint estimation. In *Proceedings of the IEEE/CVF Conference on Computer Vision and Pattern Recognition Workshops*, pages 996–997, 2020.
- [58] Yongjian Chen, Lei Tai, Kai Sun, and Mingyang Li. Monopair: Monocular 3d object detection using pairwise spatial relationships. In *Proceedings of the IEEE/CVF Conference on Computer Vision and Pattern Recognition (CVPR)*, June 2020.
- [59] Peixuan Li, Huaici Zhao, Pengfei Liu, and Feidao Cao. Rtm3d: Real-time monocular 3d detection from object keypoints for autonomous driving. In *European Conference on Computer Vision*, pages 644–660. Springer, 2020.
- [60] Xinzhu Ma, Shinan Liu, Zhiyi Xia, Hongwen Zhang, Xingyu Zeng, and Wanli Ouyang. Rethinking pseudo-lidar representation. In *Computer Vision—ECCV 2020: 16th European Conference, Glasgow, UK, August 23–28, 2020, Proceedings, Part XIII 16*, pages 311–327. Springer, 2020.
- [61] Mingyu Ding, Yuqi Huo, Hongwei Yi, Zhe Wang, Jianping Shi, Zhiwu Lu, and Ping Luo. Learning depth-guided convolutions for monocular 3d object detection. In *Proceedings of the IEEE/CVF Conference on computer vision and pattern recognition workshops*, pages 1000–1001, 2020.
- [62] Li Wang, Liang Du, Xiaoqing Ye, Yanwei Fu, Guodong Guo, Xiangyang Xue, Jianfeng Feng, and Li Zhang. Depth-conditioned dynamic message propagation for monocular 3d object detection. In *Proceedings of the IEEE/CVF Conference on Computer Vision and Pattern Recognition*, pages 454–463, 2021.

- [63] Garrick Brazil, Gerard Pons-Moll, Xiaoming Liu, and Bernt Schiele. Kinematic 3d object detection in monocular video. In *Computer Vision–ECCV 2020: 16th European Conference, Glasgow, UK, August 23–28, 2020, Proceedings, Part XXIII 16*, pages 135–152. Springer, 2020.
- [64] Xuepeng Shi, Qi Ye, Xiaozhi Chen, Chuangrong Chen, Zhixiang Chen, and Tae-Kyun Kim. Geometry-based distance decomposition for monocular 3d object detection. In *Proceedings of the IEEE/CVF International Conference on Computer Vision (ICCV)*, pages 15172–15181, October 2021.
- [65] Patrick Ruhkamp, Daoyi Gao, Hanzhi Chen, Nassir Navab, and Benjamin Busam. Attention meets geometry: Geometry guided spatial-temporal attention for consistent self-supervised monocular depth estimation. In *2021 International Conference on 3D Vision (3DV)*, pages 837–847, 2021. doi: 10.1109/3DV53792.2021.00092.
- [66] Yunpeng Zhang, Jiwen Lu, and Jie Zhou. Objects are different: Flexible monocular 3d object detection. In *Proceedings of the IEEE/CVF Conference on Computer Vision and Pattern Recognition*, pages 3289–3298, 2021.
- [67] Yan Lu, Xinzhu Ma, Lei Yang, Tianzhu Zhang, Yating Liu, Qi Chu, Junjie Yan, and Wanli Ouyang. Geometry uncertainty projection network for monocular 3d object detection. In *Proceedings of the IEEE/CVF International Conference on Computer Vision*, pages 3111–3121, 2021.
- [68] Xuan He, Fan Yang, Kailun Yang, Jiacheng Lin, Haolong Fu, Meng Wang, Jin Yuan, and Zhiyong Li. Ssd-monodetr: Supervised scale-aware deformable transformer for monocular 3d object detection. *IEEE Transactions on Intelligent Vehicles*, 2023.